PHYSICAL REVIEW B **95**, 184414 (2017)

# Antiferromagnetic structure and electronic properties of $BaCr_2As_2$ and $BaCrFeAs_2$

Kai A. Filsinger,[1] Walter Schnelle,[1] Peter Adler,[1] Gerhard H. Fecher,[1] Manfred Reehuis,[2] Andreas Hoser,[2]
Jens-Uwe Hoffmann,[2] Peter Werner,[3] Martha Greenblatt,[4] and Claudia Felser[1]
[1]*Max Planck Institute for Chemical Physics of Solids, Nöthnitzer Straße 40, 01187 Dresden, Germany*
[2]*Helmholtz-Zentrum Berlin für Materialien und Energie, 14109 Berlin, Germany*
[3]*Max Planck Institute of Microstructure Physics, Weinberg 2, 06120 Halle (Saale), Germany*
[4]*Department of Chemistry and Chemical Biology, Rutgers University, Piscataway, New Jersey, USA*
(Received 9 January 2017; published 12 May 2017)

Recent theoretical studies suggest that superconductivity may be found in doped chromium pnictides with crystal structures similar to their iron counterparts. Here, we report a comprehensive study on the magnetic arsenides $BaCr_2As_2$ and $BaCrFeAs_2$ (space group $I4/mmm$), which are possible mother compounds with $d^4$ and $d^5$ electron configurations, respectively. DFT-based calculations of the electronic structure evidence metallic antiferromagnetic ground states for both compounds. By powder neutron diffraction, we confirm for $BaCr_2As_2$ a robust ordering in the antiferromagnetic $G$-type structure at $T_N = 580$ K with $\mu_{Cr} = 1.9\,\mu_B$. Anomalies in the lattice parameters point to magnetostructural coupling effects. In $BaCrFeAs_2$, the Cr and Fe atoms randomly occupy the transition-metal site and $G$-type order is found below 265 K with $\mu_{Cr/Fe} = 1.1\,\mu_B$. $^{57}$Fe Mössbauer spectroscopy demonstrates that only a small ordered moment is associated with the Fe atoms, in agreement with electronic structure calculations leading to $\mu_{Fe} \sim 0$. The temperature dependence of the hyperfine field does not follow that of the total moments. Both compounds are metallic but show large enhancements of the linear specific heat. Electrical transport in $BaCrFeAs_2$ is dominated by the atomic disorder and the partial magnetic disorder of Fe. Our results indicate that Néel-type order is unfavorable for Fe moments and thus it is destabilized with increasing Fe content.

DOI: 10.1103/PhysRevB.95.184414

## I. INTRODUCTION

Intense efforts are made to investigate and theoretically model the magnetic states adopted by the nonsuperconducting relatives of the iron-based pnictide and chalcogenide high-$T_c$ superconductors [1–3]. Similar as for the oxocuprate superconductors, there is a subtle interplay between magnetism and superconductivity (sc), and spin fluctuations are considered as the mechanism enabling the formation of Cooper pairs [4]. The possible coexistence of specific types (spin-density wave, SDW) of magnetic order and sc on the microscale in the Fe-based systems is an ongoing topic of research.

The antiferromagnetic (AFM) parent compounds of cuprate superconductors are Mott (charge transfer) insulators. The situation is less clear for their Fe-based counterparts. For instance, nonsuperconducting pnictides like LaOFeAs or $BaFe_2As_2$ are metallic, itinerant antiferromagnets with low ordered moments at the iron sites ($< 1\,\mu_B$), whereas chalcogenides like $K_{0.8}Fe_{1.6}Se_2$ are insulators with large Fe moments of $\approx 3\,\mu_B$. Strictly, half-filled systems with $d^5$ configuration may be regarded as the Mott-type parent compounds, which is confirmed by the semiconducting properties of, e.g., $BaMn_2As_2$ [5–9] and LaOMnAs and LiMnAs [10,11].

The proper description of the electronic structure of Fe-based pnictides and chalcogenides, in particular the importance of electron correlation and the degree of electron itinerancy is under debate [12,13]. Since the basic Fe-As layers with formally $Fe^{2+}$ ions in the parent compounds constitute a multiorbital system, orbital ordering is believed to be of importance. Two opposing views have been adopted: (i) the iron pnictides have been considered as weakly correlated metals where a SDW magnetic state is formed due to Fermi surface nesting and (ii) the more strongly correlated selenides have been discussed as Mott-type insulators and the magnetism was modeled in terms of Heisenberg-type exchange interactions between localized moments. However, none of the limiting views can describe the many facets of magnetism, which have emerged from experiments and actually it is believed that the Fe-based pnictides and chalcogenides are in between these extremes. For instance, even itinerant electronic systems may show pronounced correlation effects arising from Hund's rule coupling (Hund's metals [3,14]), which rationalizes the existence of large magnetic moments on short time scales [13].

An important prototype system is $BaFe_2As_2$, which adopts the tetragonal $ThCr_2Si_2$-type crystal structure at room temperature and features a structural/magnetic transition at $T_N = 132$ K [15]. Below $T_N$, a stripelike AFM order occurs with saturated Fe moments of $\approx 0.9\,\mu_B$ aligned along the $a$ axis of the low-$T$ orthorhombic crystal structure [16]. $BaFe_2As_2$ can be converted into a high-$T_c$ superconductor by hole or electron doping [15,17,18] or by high pressure [19]. While substitution of Fe by some transition metals like Co, Ni, or even Ru [20–22] induces sc, substitution by others like Mn does not lead to sc states [23]. In contrast to $BaFe_2As_2$, the half-filled analog $BaMn_2As_2$ remains tetragonal and adopts a $G$-type AFM spin structure (i.e., both intra and interplane couplings are AFM) with a large ordered moment ($3.9\,\mu_B$) and a high Néel temperature of 625 K [7,8]. Similarly, high-$T_N$ (692–758 K) and $G$-type AFM have been observed for Cr species in isostructural silicides $RCr_2Si_2$ ($R =$ Tb, Ho, and Er) [24].

The Mott scenario for the transition-metal arsenides [25] considers a mirror symmetry in the many-body physics arising when the half-filled $d^5$ configuration is either doped by electrons or by holes. The Cr compounds formally have a $d^4$

configuration and in this sense are the hole-doped analogues to the $d^6$ system $BaFe_2As_2$. Recently, theoretical studies explored the possibilities to find sc for $BaM_2As_2$ and LaO$M$As with transition metals $M$ (or mixtures) with less than five electrons [26,27]. In these works the correlation strength in dependence of the band filling is investigated and compared to that in actual Fe-based superconductors. Superconductivity in Cr and Mn compounds is rare and only recently some representatives have been found [28–32].

Here, we focus on the system $Ba(Fe_{1-x}Cr_x)_2As_2$, where no sc compositions have been found so far [23,33,34]. Theoretical calculations predicted an AFM checkerboard ($G$-type) ordering in $BaCr_2As_2$ [35] and a ferromagnetic (FM) state in atomically ordered $BaCrFeAs_2$ [7]. Another electronic structure calculation predicted ordered $BaCrFeAs_2$ as a fully compensated antiferromagnet with an iron moment of $2.6\,\mu_B$ [36]. Such a material could be relevant for spintronics applications. Neutron diffraction studies on Fe-rich $BaFe_{2-x}Cr_xAs_2$ single crystals with $0 < x < 0.94$ indicated that near $x = 0.6$ the SDW is replaced by a $G$-type AFM state [34]. The spin structure and ordering temperature of the end member $BaCr_2As_2$ have not been studied experimentally yet. Electronic structure calculations of $EuCr_2As_2$ suggested also a stable $G$-type AFM order of the Cr sublattice. This and the FM ordering of the $Eu^{2+}$ ions at 21 K was confirmed experimentally [37,38].

We investigate the crystal and magnetic structures of $BaCr_2As_2$ and $BaCrFeAs_2$ by temperature dependent powder neutron diffraction. Our theoretical studies predict a random occupation of Cr and Fe on the transition-metal site for $BaCrFeAs_2$ and metallic AFM $G$-type order for both compounds. Experimentally, both compounds in fact feature $G$-type AFM order, where the Néel temperature $T_N = 580$ K of $BaCr_2As_2$ is nearly as high as that of $BaMn_2As_2$. Both compounds are metallic conductors. $BaCrFeAs_2$ is atomically disordered and thus only average magnetic moments are obtained from neutron diffraction. Most interestingly, the Fe Mössbauer spectra indicate that the Fe moments are much smaller than those of Cr and of similar size as in $BaFe_2As_2$. $T_N$ decreases with increasing Fe content, thus $G$-type order is unfavorable for Fe moments. The itinerant character of the magnetism persists in the whole stability range of the $G$-type order, whereas $BaMn_2As_2$ with the same nominal $d$ electron count as $BaCrFeAs_2$ is a semiconductor.

## II. EXPERIMENTAL & CALCULATION DETAILS

$BaCr_2As_2$ and $BaCrFeAs_2$ were synthesized by reacting CrAs and FeAs with Ba in an alumina crucible. The binaries were synthesized according to Singh *et al.* [35] using Cr (chemPUR, 99.99 %), Fe (chemPUR, 99.9 %), and As (Alfa Aesar, 99.999 %). To control the harsh reaction between the binaries and Ba (Alfa Aesar, 99.999 %), only 1/3 of the barium was added initially. The mixture was heated to 1423 K and held for 12 h. Then the product was ground and additional Ba was added. These steps were repeated until the powder x-ray diffraction (PXRD) pattern did not show any CrAs or FeAs impurities. In both cases an excess of ≈ 5 % Ba was added to react all of the strongly magnetic CrAs or FeAs. Single crystals were grown using the Bridgman technique with alumina crucibles under argon atmosphere. The crucible was heated to 1823 K and held for 24 h, then it was moved with 1 mm $h^{-1}$ out of the hot zone of the furnace. $BaCr_2As_2$ crystals [Fig. 1(b)] up to 10×5×4 mm could be grown ($BaCrFeAs_2$ crystals were much smaller). For the neutron diffraction experiments, ≈ 4 g of powder was used.

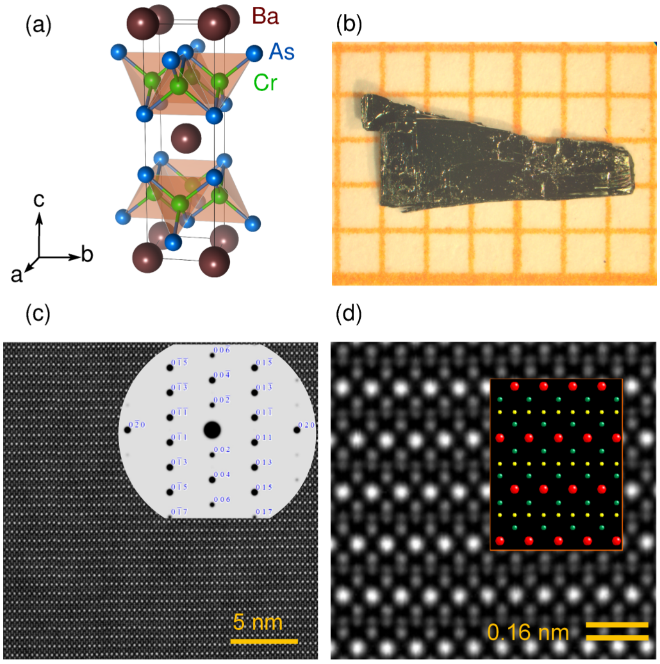

FIG. 1. (a) $BaCr_2As_2$ crystallizes in the $ThCr_2Si_2$ structure (space group $I4/mmm$). (b) Crystals form as shiny black platelets. (c) HAADF image and diffraction pattern. (d) Zoom of the HAADF image, the inset shows the theoretical atom positions (Ba red, Cr green, and As yellow).

The crystal structure [$ThCr_2Si_2$ type, $tI10$, space group (SG) $I4/mmm$, No. 139, Ba on $2a$, Cr on $4d$, As on $4e$] was confirmed by PXRD using Cu-$K_\alpha$ radiation ($\lambda = 1.54056$ Å), with a Huber G670 camera (Guinier technique). The refined lattice parameters are $a = 3.9667$ and $c = 13.6214$ Å for $BaCr_2As_2$ and $a = 3.986$ and $c = 13.2939$ Å for $BaCrFeAs_2$. Additional reflexes suggest the presence of traces of $BaAl_2O_4$ in some samples. High-resolution transmission electron microscopy (HR-TEM) microstructure studies were performed using a FEI Titan 80-300. In the high-angle annular dark field (HAADF) images [shown in Figs. 1(c) and 1(d)] for $BaCr_2As_2$; not shown for $BaCrFeAs_2$) no signs of disorder on the Ba $2a$(0,0,0), Cr/(CrFe) $4d$ ($\frac{1}{2}$,$\frac{1}{2}$,$\frac{1}{2}$), or As $4e$ (0,0,$z$) sites could be found. In agreement with the PXRD pattern, segregates of $BaAl_2O_4$ were seen on the surface for some $BaCrFeAs_2$ crystals. The average composition of the crystals was found to be $Ba_{1.03(4)}Cr_{2.01(5)}As_{2.03(5)}$ and $Ba_{1.01(6)}Cr_{0.96(8)}Fe_{1.08(2)}As_{2.10(1)}$ by chemical analysis with inductively coupled plasma optical emission spectroscopy (ICP-OES).

Powder neutron diffraction experiments on $BaCr_2As_2$ and $BaCrFeAs_2$ have been carried out on the instruments E2, E6, and E9 at the BER II reactor of the Helmholtz-Zentrum Berlin. Fine powders were placed in a vanadium cylinder of 4 mm diameter and 40 mm length. The fine-resolution instrument E9 uses a Ge-monochromator selecting the neutron wavelength $\lambda = 1.7973$ Å, while the instruments E2 and E6 (with higher neutron flux but lower resolution) use a pyrolytic graphite monochromator selecting the wavelength $\lambda = 2.38$ and 2.42 Å, respectively. On these instruments powder patterns were recorded in the following ranges of diffraction angles: $7.7^\circ \leqslant 2\theta \leqslant 83.4^\circ$ (E2), $7.5^\circ \leqslant 2\theta \leqslant 136.5^\circ$ (E6), and $8^\circ \leqslant 2\theta \leqslant 141^\circ$ (E9). In case of $BaCr_2As_2$, powder patterns were collected between 2 and 750 K, for $BaCrFeAs_2$ between 2 and 275 K. The refinements of the crystal and magnetic structure were carried out with FULLPROF [39] using Pseudo-Voigt functions and the nuclear scattering lengths $b(O) = 5.805$ fm, $b(Cr) = 3.635$ fm, $b(Fe) = 9.54$ fm, and $b(Ba) = 5.25$ fm [40]. The magnetic form factors of the $Cr^{3+}$ and $Fe^{3+}$ ions were taken from Ref. [41].

Magnetization was measured in two magnetometer systems (MPMS-XL7 and MPMS3 with oven, Quantum Design). For some crystals small differences were seen between data taken in warming after zero-field cooling (zfc) and during cooling in field (fc). Such differences seem to be due to tiny CrAs precipitations (see below). Electrical resistivity, magnetoresistance, Hall effect, and heat capacity were determined with a measurement system (ACT and HC options, PPMS9, Quantum Design).

Mössbauer spectra of $BaCrFeAs_2$ were measured with a standard WissEl spectrometer and a Janis closed cycle refrigerator (SHI-850-5) using a $^{57}Co/Rh$ source and a drive system operating in constant acceleration mode. The Mössbauer absorber consisted of an acrylic glass sample container with a sample density of $\approx 17$ mg per cm$^2$. In order to ensure homogeneous distribution the sample was mixed with boron nitride. Spectra were collected between 5 and 292 K and evaluated with MossWinn [42]. Hyperfine field distributions were extracted using the Hesse-Rübartsch method. Isomer shifts are given relative to $\alpha$-iron.

The electronic structures were calculated self-consistently in the local spin density approximation (LSDA) using the full potential linearized augmented plane wave (FLAPW) method including spin-orbit (SO) interaction as implemented in WIEN2k [43–45]. For atomically disordered $BaCrFeAs_2$ the calculations were carried out using the full potential, spin polarized relativistic Korringa-Kohn-Rostocker method (SPRKKR) [46,47]. In all calculations the PBE exchange-correlation functional [48] and the generalized gradient approximation (GGA) was used. To estimate the influence of a static correlation, the LDA + $U$ method was applied.

For $BaCr_2As_2$, the calculations were started with the values $a = 3.96$ Å, $c = 13.6$ Å, and $z = 0.361$ [49]. A $G$-type AFM order was assumed and the lattice was set up in SG $I\bar{4}m2$ (No. 119) and the Cr atoms were located on the split $2c$ and $2d$ sites to allow for the anti-parallel orientations of their magnetization. This space group concerns the atomic positions, the final magnetic symmetry depends on the direction of the quantization axis and is described by a Shubnikov color group [here $P\,4'/m'm'm$ (123.344)]. A full structural optimization showed that the above given parameters are nearly relaxed, in agreement with previous observations [35].

In the calculations of the electronic structure for $BaCrFeAs_2$, the same basic atomic and magnetic structures were used. Two cases were assumed, an ordered and an alloyed structure. In the ordered structure, the initial $4d$ position of the Cr atom was split and half of the new positions was occupied by Fe. This results in SG $I\bar{4}2m$ (No. 119) with Ba $2a$, Cr $2c$, Fe $2d$, and As $4e$. Starting from the experimental lattice parameters, an optimization of the ordered structure resulted in $a_{\text{opt}} = 4.012$ Å, $c_{\text{opt}} = 13.3819$ Å, and $z_{\text{opt}} = 0.357$. The strong deviations of these optimized parameters from the experimental ones suggest that the ordered case is not realized, i.e., in the actual material, Cr and Fe are disordered. For the alloyed structure, it was assumed that Fe and Cr occupy both the $2c$ and $2d$ position in a 50:50 ratio.

## III. RESULTS

### A. Crystal structures

The crystal structures of $BaCr_2As_2$ and $BaCrFeAs_2$ were investigated by powder neutron diffraction. Below $T_N = 580$ K, respectively 265 K, the patterns also included magnetic Bragg intensity (see Sec. III E). Both compounds crystallize in the tetragonal SG $I4/mmm$ (No. 139), where the Ba, Cr(Fe), and As atoms occupy the Wyckoff positions $2a(0,0,0)$, $4d(0,\frac{1}{2},\frac{1}{4})$, and $4e(0,0,z)$, respectively. The same SG was reported earlier for $BaMn_2As_2$ [6]. From the data sets collected on the fine-resolution powder diffractometer E9 we could not find any additional peak splitting indicating a lower crystal structure symmetry. The refinements of the crystal structure of $BaCr_2As_2$ from data sets recorded in the temperature range from 2 up to 750 K resulted in residuals between $R_N = 0.048$ and 0.088 [defined as $R_N = (\Sigma||F_{\text{obs}}| - |F_{\text{calc}}||)/\Sigma|F_{\text{obs}}|$]. These values are somewhat larger than expected. This can be ascribed to the fact, that the investigated sample contained an impurity, which could not be characterized so far (see Fig. 2). Additional impurity peaks of the sample container were observed in the diffraction patterns using the furnace on E9. Nevertheless, the lattice parameters, as well as the positional parameters of $BaCr_2As_2$ could be refined with good accuracy. The crystal structure of $BaCrFeAs_2$ was investigated in the range 2–275 K. Due to the high purity of this sample the refinements resulted in residuals between $R_N = 0.035$ and 0.043. The results of the Rietveld refinements of the data sets collected at 2 K are given in Table I. It is emphasized that there are no indications of superstructure reflections which would point to atomic order of Cr and Fe atoms.

Figure 3(a) shows the temperature dependence of the cell parameters as well as the cell volume. For $BaCrFeAs_2$, the parameters $a$ and $c$ show a continuous increase from 2 up to 275 K, which is above the magnetic ordering temperature $T_N = 265(5)$ K. A similar trend was found for $BaMn_2As_2$ [6]. A continuous increase of $a$ and $b$ was also observed for $BaCr_2As_2$ but only in the range 2–300 K. Further heating up to 700 K leads to a decrease of $c$, while the increase of $a$ becomes somewhat more pronounced (see Fig. 3). As a consequence, the ratio $c/a$ decreases from 3.43 at 300 K to 3.34 at 750 K. The former value is in agreement with Ref. [49]. These results indicate that the magnetic transition in $BaCr_2As_2$ is accompanied by subtle structural modifications, in contrast to $BaMn_2As_2$ [6]. The anomaly in the $c$ parameter is reflected in the change of the distance between the arsenic atoms lying along the $c$ direction. Namely, one observes a decrease of the distance $d$(As-As) between about 300 K and

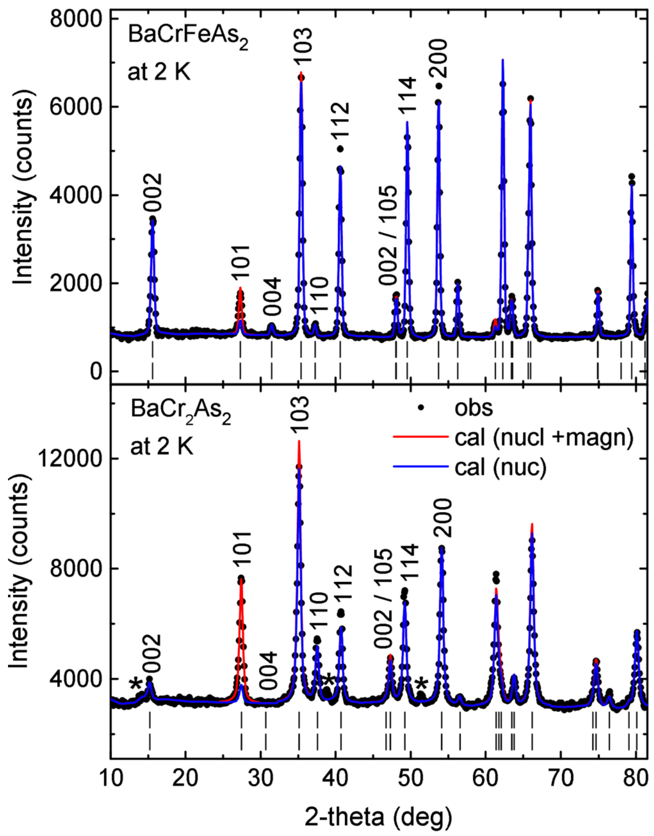

FIG. 2. Neutron diffraction patterns of $BaCr_2As_2$ and $BaCrFeAs_2$ powder taken at $T = 2$ K. The calculated patterns of the pure nuclear contribution (blue) as well as the sum of the nuclear and the magnetic contribution (red) are compared with the observed ones (black full circles). In the lower part, the positions of the Bragg peaks are given (black ticks). The $BaCr_2As_2$ sample contained an impurity (positions marked with $*$), which could not be identified so far.

the Néel temperature $T_N = 580(10)$ K as shown in Fig. 4. Above $T_N$ finally $d$(As-As) seems to show a slight increase up to 750 K. The bond length $d$(Cr-As) only shows a slight increase from 2 K up to 750 K, but a weak anomaly is observed near $T_N$. In contrast, in $BaCrFeAs_2$ both $d$(As-As) and $d$(Cr-As) only show a slight increase in the range 2–275 K without anomalies, indicating that magnetic ordering does not influence the structural properties significantly. In Fig. 4, we have also plotted the changes of the two different bond angles $\angle_1$(As-Cr-As) and $\angle_2$(As-Cr-As) in the $CrAs_4$ (and $Cr/FeAs_4$) tetrahedra, which form a twodimensional layer in the *ab* plane. The structural anomalies accompanying the magnetic transition in $BaCr_2As_2$ are also reflected in the bond angles. Thus $\angle_1$(As-Cr-As) and $\angle_2$(As-Cr-As) show a strong increase and decrease in the magnetically ordered state. Above 650 K both angles seem to reach saturation values. In contrast, the two bond angles for $BaCrFeAs_2$ are practically unchanged between 2 and 275 K. However, both pnictides do not reach the ideal tetrahedron angle of 109.47°. The tetrahedra in $BaCr_2As_2$ are stronger distorted than those in $BaCrFeAs_2$.

### B. Electronic structure of $BaCr_2As_2$

In Fig. 5, the Fermi surface of $BaCr_2As_2$ is shown. Three bands are crossing the Fermi energy $\epsilon_F$, resulting in three isosurfaces. The innermost one is closed and has a cushion shape. It is related to a hole pocket around the $\Gamma$ point. The outer two are open at top and bottom and have corrugated cylinder shapes with fourfold arranged bulges. The effective band mass $m^\star/m_e$ of the innermost hole pocket was determined for the $\Delta$ and $\Sigma$ directions revealing values of $m^\star_\Delta = -0.63$ and $m^\star_\Sigma = -0.39$ at the $\Gamma$ point. This hints that this band is in the GGA-LSDA not responsible for the observed enhanced value of the electronic specific heat coefficient $\gamma$ (cf. Ref. [35] and our specific heat results in Sec. III D).

TABLE I. Results of the crystal structure refinements for $BaCr_2As_2$ and $BaCrFeAs_2$. The refinements of the powder neutron diffraction data (instrument E9) were carried out in the tetragonal space group $I4/mmm$. The isotropic temperature factors of the atoms were constrained to be equal [50].

| $BaCr_2As_2$ at $T = 2$ K, $R_N = 0.048$<br>$a = 3.9503(2)$ Å, $c = 13.6047(10)$ Å, $Z = 2$, $V = 212.30(3)$ Å$^3$ | | | | | |
|---|---|---|---|---|---|
| atom | site | $x$ | $y$ | $z$ | $B$ (Å$^2$) |
| Ba | $2a$ | 0 | 0 | 0 | 0.32(3) |
| Cr | $4d$ | 0 | $\frac{1}{2}$ | $\frac{1}{4}$ | 0.32(3) |
| As | $4e$ | 0 | 0 | 0.36092(14) | 0.32(3) |
| $BaCrFeAs_2$ at $T = 2$ K, $R_N = 0.040$<br>$a = 3.9793(1)$ Å, $c = 13.2532(4)$ Å, $Z = 2$, $V = 209.86(1)$ Å$^3$ | | | | | |
| atom | site | $x$ | $y$ | $z$ | $B$ (Å$^2$) |
| Ba | $2a$ | 0 | 0 | 0 | 0.19(2) |
| Cr | $4d$ | 0 | $\frac{1}{2}$ | $\frac{1}{4}$ | 0.19(2) |
| Fe | $4d$ | 0 | $\frac{1}{2}$ | $\frac{1}{4}$ | 0.19(2) |
| As | $4e$ | 0 | 0 | 0.35779(10) | 0.19(2) |

The evolution of the DOS with increasing Coulomb parameter $U$ in the LDA + $U$ calculation is given in Fig. 6. Note that the unoccupied minority states of one of the Cr atoms correspond to the unoccupied majority states of the other, and vice versa for the occupied states due to the anti-symmetric spin densities of an antiferromagnet. The increased $U$ results in an increase of the magnetic moment at the Cr atoms (cf. Table II). Their values are in the range 2.4–3.5 $\mu_B$.

The "bare" coefficient of the electron specific heat $\gamma_0 = \pi^2 k_B^2 n(\epsilon_F)/3$ for $BaCr_2As_2$ is $\approx 8$ mJ mol$^{-1}$ K$^{-2}$. For the various calculation schemes the results are also given in Table II. The inclusion of SO interaction has only a weak effect on $\gamma_0$. For LDA + $U$, it is found that $n(\epsilon_F)$—and thus $\gamma_0$—increases slightly and has a maximum at $U \approx 1$ eV, but then decreases with further increase of $U$. A Néel temperature of $T_{N,calc} \approx 880$ K is determined in the mean field approximation using the calculated exchange parameters from SPRKKR.

### C. Electronic structure of $BaCrFeAs_2$

The electronic structure of the ordered variant of $BaCrFeAs_2$ should be a completely compensated half-metallic ferrimagnet as reported in Ref. [36]. The peculiarity of this type of magnetism is that the moment of two different types of atoms—here Cr and Fe—compensate each other similar to a antiferromagnet. The different symmetry, however, allows that the DOS in the two spin channels are different. Moreover,

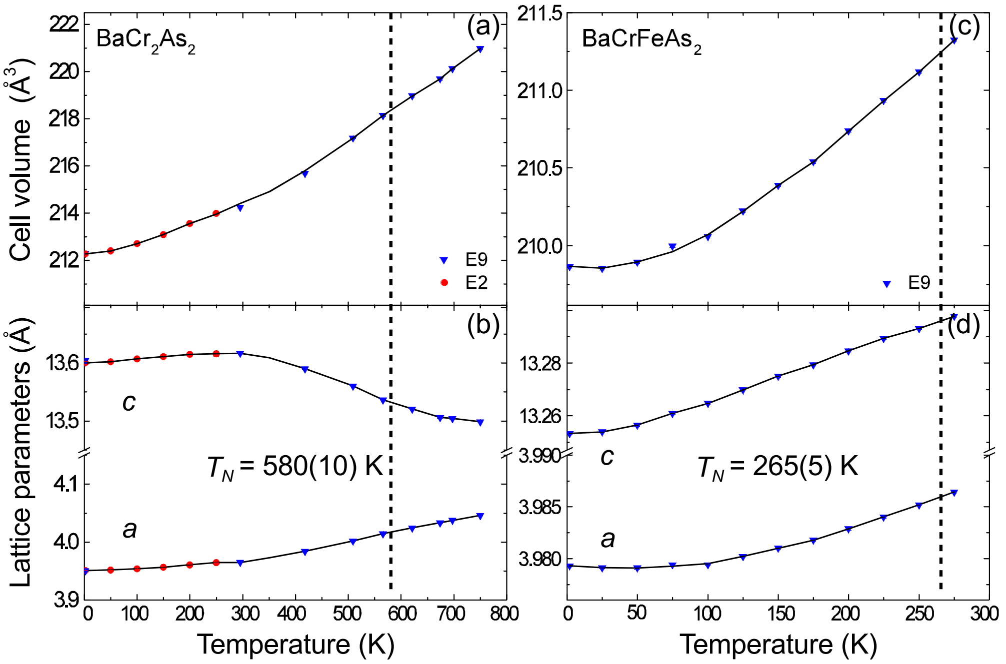

FIG. 3. Temperature dependence of the lattice parameters and the cell volumes of BaCr$_2$As$_2$ and BaCrFeAs$_2$. These values were determined from data sets collected on the instruments E2 and E9.

a band gap at $\epsilon_F$ appears in one of the spin densities similar to a half-metallic ferromagnet. The DOS for the $\uparrow$ spin channel has a pronounced maximum just above $\epsilon_F$ with a value of $n(\epsilon_F + \delta) = 6.92$ eV$^{-1}$ ($\delta \approx 50$ meV). This value is twice as high as the one calculated for BaCr$_2$As$_2$. It arises from flat bands around $\epsilon_F$. A detailed analysis of the DOS reveals that those states are localized at the Fe atoms. In many cases, compounds with such a peaked DOS at $\epsilon_F$ are not stable.

The electronic structure and the DOS of the alloy variant of BaCrFeAs$_2$ are shown in Fig. 7. The result of the chemical disorder scattering are strongly broadened electronic states, in particular close to $\epsilon_F$. The broadening causes a reduction of the maximum of the DOS just above $\epsilon_F$ to about 5 eV$^{-1}$, which is still higher compared to BaCr$_2$As$_2$. The magnetic properties of ordered and alloyed BaCrFeAs$_2$ are compared in Table III. The moment for the atomically ordered phase compares well with 2.6 $\mu_B$ reported in Ref. [36]. The moments in the ordered case are not completely the same, the vanishing total moment is guaranteed by the polarization of the interstitial and the atoms in the vicinity of the magnetic Cr and Fe atoms. The orbital magnetic moments are very small, in the order of 0.002 $\mu_B$ or 0.06 $\mu_B$.

Interestingly, for the random distribution of Fe and Cr, a stable solution is found with vanishing moments at the Fe atoms at the same site. The calculation was started with a starting moment at the Cr atoms (4 $\mu_B$) but zero moment at Fe. No magnetic moment was induced during the self consistent cycles. The result is an average moment of 1.38 $\mu_B$ for the $2c/2d$ positions.

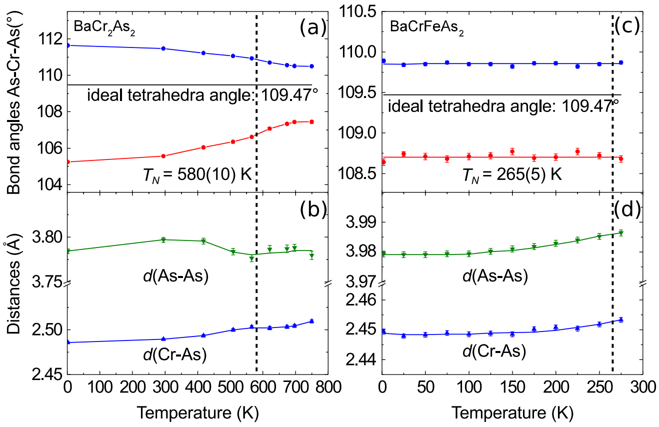

FIG. 4. Temperature dependence of the interatomic distances $d$(Cr-As) and $d$(As-As) and of the bond angles $\angle_1$(As-Cr-As) (blue) and $\angle_2$(As-Cr-As) (red) in the CrAs$_4$ tetrahedron for BaCr$_2$As$_2$. These and the corresponding values for BaCrFeAs$_2$ were refined from data taken on instrument E9.

Also, for BaCrFeAs$_2$, the Néel temperature can be calculated in the mean-field approximation using SPRKKR.

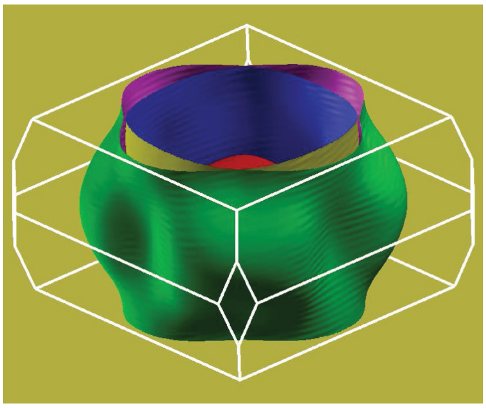

FIG. 5. Fermi surface of BaCr$_2$As$_2$.

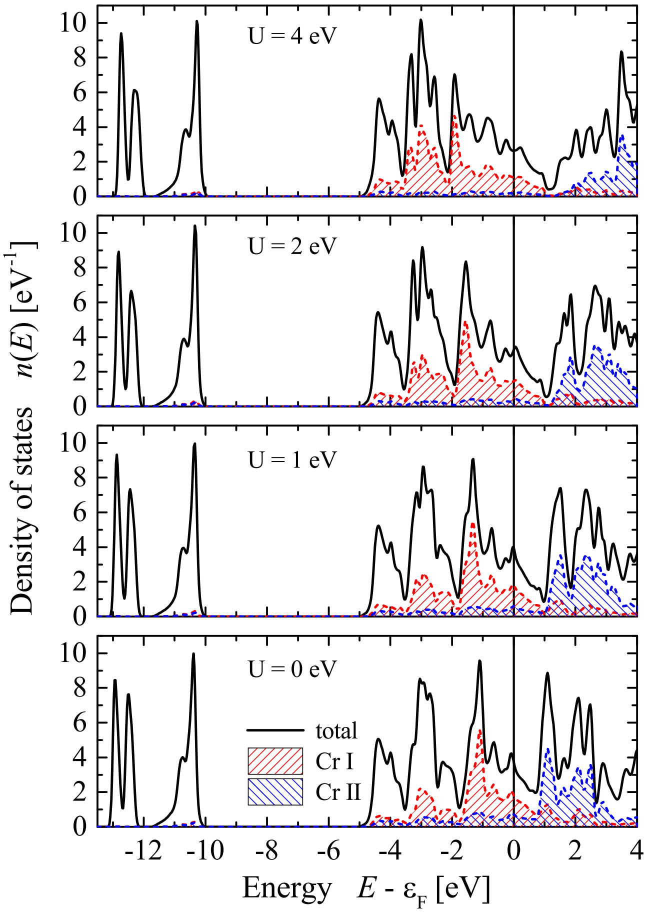

FIG. 6. Density of states of $BaCr_2As_2$ calculated with LDA + $U$. Shown is the total DOS together with the local DOS at Cr atoms for increasing $U$.

The value for the atomically ordered structure is very high, however, a much lower Néel temperature of about 260 K is obtained for the disordered version.

### D. Magnetic and thermal properties, electrical transport

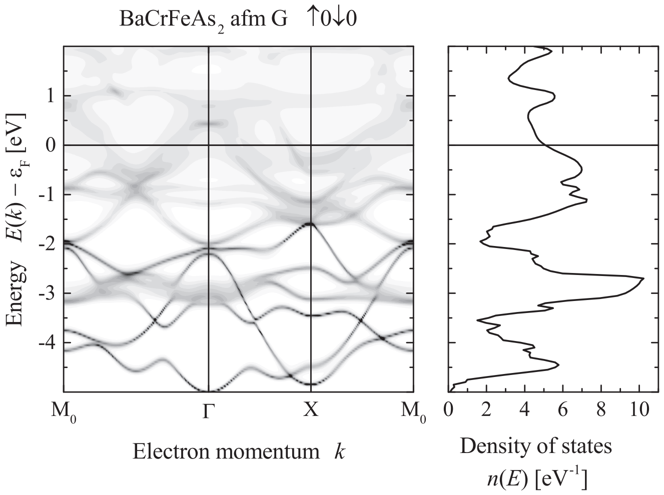

FIG. 7. Electronic structure of $BaCrFeAs_2$ with chemical disorder between Cr and Fe. Shown is the case with a vanishing magnetic moment at Fe. The DOS is the same in both spin channels due to the AFM order, thus the sum is plotted.

The temperature dependence of the magnetic susceptibility, $\chi = M/H$, at $\mu_0 H = 1$ T of a $BaCr_2As_2$ crystal platelet (*ab* plane) was measured with the magnetic field parallel and perpendicular to the $c$ axis (Fig. 8). The small difference between the directions above 600 K suggests a rather weak anisotropy in the paramagnetic regime. However, no Curie-Weiss behavior could be observed up to $T = 800$ K. For $H \parallel c$, a clear kink is visible, indicating the AFM ordering of the Cr sublattice at $T_N = 575(10)$ K, as determined from the peak in the derivative $d(\chi T)/dT$. The decrease of $\chi(T)$ for $H \parallel c$ towards low temperatures is much stronger than for $H \perp c$, eventually suggesting an AFM order with magnetic moments aligned along the $c$ axis. The behavior of $\chi(T)$ and the ordering temperature is very similar to that of $BaMn_2As_2$ [8]. The nearly isotropic but non-Curie-Weiss behavior above $T_N$ is observed for several AFM compounds with $ThCr_2Si_2$-type structure. It is typical for the somewhat twodimensional character of the magnetic interactions and has been treated in detail theoretically for $BaMn_2As_2$ [8]. For $BaCr_2As_2$, the smooth maximum of $\chi(T)$ may be anticipated for temperatures around 900 K.

A small upturn of $\chi(T)$ in both directions for temperatures below ≈ 50 K suggests the presence of paramagnetic impurities, e.g., from point defects. Magnetization loops taken at $T = 1.8$ K (Fig. 8 inset) show a very small FM-like component of $< 5\times10^{-4}\mu_B$ for both field along or perpendicular to the $c$ axis. Also, in measurements of $M(T)$ at $\mu_0 H = 0.01$ T, a small sharp transition from a FM impurity phase becomes visible at

TABLE II. Spin magnetic moment of the Cr atoms, the DOS at the Fermi energy $n(\epsilon_F)$, and the coefficient of the electron specific heat $\gamma_0$ for different calculation schemes for $G$-type AFM ordered $BaCr_2As_2$. All calculations were performed including spin-orbit interaction (SO).

| method | $U$ eV | $m_{Cr}$ $\mu_B$ | $n(\epsilon_F)$ $eV^{-1}$ | $\gamma_0$ mJ $mol^{-1}$ $K^{-2}$ |
|---|---|---|---|---|
| GGA with SO | 0 | 2.4 | 3.37 | 7.95 |
| LDA + $U$ | 1 | 2.8 | 3.67 | 8.65 |
| | 2 | 3.1 | 2.45 | 5.77 |
| | 3 | 3.3 | 2.91 | 6.85 |
| | 4 | 3.4 | 2.85 | 6.71 |
| | 5 | 3.5 | 1.84 | 4.35 |

TABLE III. Magnetic properties of $BaCrFeAs_2$. Tabulated are the DOS just above $\epsilon_F$ ($n_{max}$), the absolute values of the magnetic moments at Cr and Fe species ($m_{Cr/Fe}$), and the calculated Néel temperatures ($T_{N,calc}$).

| | ordered | disordered | |
|---|---|---|---|
| $n_{max}$ | 6.92 | 4.99 | ($eV^{-1}$) |
| $m_{Cr}$ | 2.74 | 2.76 | ($\mu_B$) |
| $m_{Fe}$ | 2.53 | 0.00 | ($\mu_B$) |
| $T_{N,calc}$ | 965 | 260 | (K) |

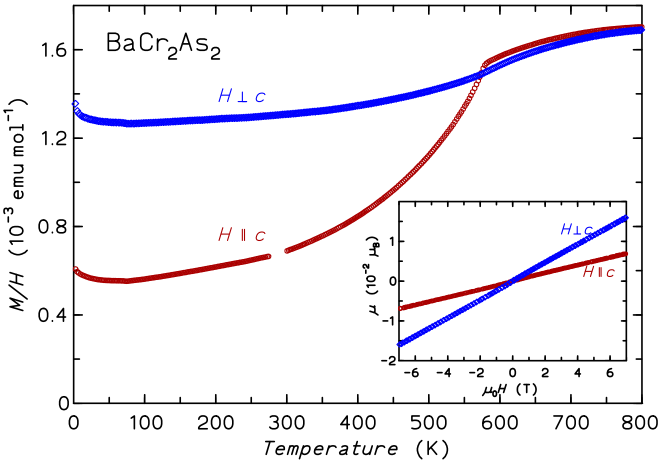

FIG. 8. Magnetic susceptibility of a BaCr$_2$As$_2$ crystal in a field $\mu_0H = 1$ T perpendicular (blue diamonds) and parallel (red circles) to the crystallographic $c$ axis. Minor adjustments of the magnetometer oven data sets ($T > 400$ K) were made to match with the data below 400 K. The inset shows the magnetic moment from an isothermal magnetization loop measured at a temperature $T = 1.8$ K.

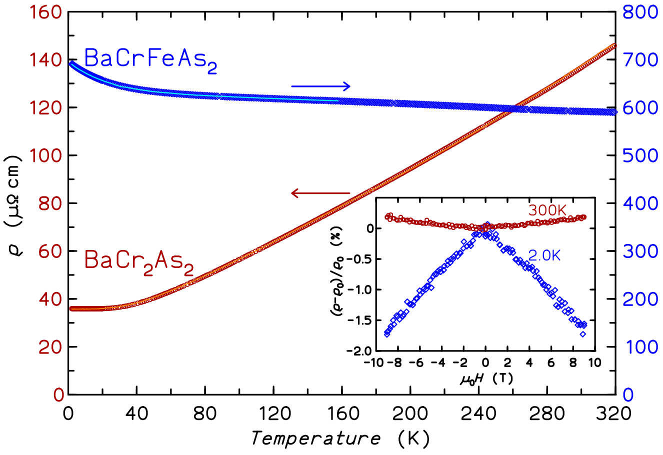

FIG. 10. Electrical resistivity of a BaCr$_2$As$_2$ crystal measured in the crystallographic $ab$ plane (red circles) and of a sintered sample of BaCrFeAs$_2$ (blue diamonds) in zero magnetic field. The resistivity curves in $\mu_0H = 9$ T (lines) almost coincide with the zero-field data. The inset shows the magnetoresistance $100\times(\rho - \rho_0)/\rho_0$ as function of field for BaCr$_2$As$_2$ measured at $T = 2.0$ and 300 K.

$T_{\mathrm{imp}} \approx 76$ K. We assign this transition and the FM-like signals to the structural and helimagnetic ordering transition of CrAs [51]. The ordering temperature of CrAs is known to decrease dramatically to zero for pressures of 0.7–0.8 GPa [28,29]. We speculate that CrAs on the crystal surface is strained and its ordering temperature is reduced to $T_{\mathrm{imp}}$.

The magnetic susceptibility of sintered BaCrFeAs$_2$ (Fig. 9) displays a broadened cusp at $T_N \approx 269(2)$ K [midpoint of step in $d(\chi T)/dT$], but there is only a slight decrease of the $\chi(T)$ curve below this temperature. Instead, with decreasing temperature the susceptibility increases again, indicating a strong paramagnetic contribution following a Curie law. Above the Néel temperature (range 300–400 K), the data are well fitted by a Curie-Weiss law with effective moment $\mu_{\mathrm{eff}} = 3.70\,\mu_B$ and Weiss temperature $\theta_P = -273$ K. The BaCrFeAs$_2$ crystal shows a similar cusp, however at $\approx 225$ K. The lower $T_N$ of the single crystal is probably due to a slightly higher Fe content compared to the sinter sample. The decrease of $\chi(T)$ is more pronounced for $H \parallel c$, suggesting an AFM ordered structure with the magnetic moments lying in the crystallographic $c$ direction. The paramagnetic contribution in the magnetically ordered state of BaCrFeAs$_2$ is discussed in connection with the Mössbauer results (Sec. III F).

The electrical resistivity, $\rho(T)$, of the BaCr$_2$As$_2$ crystal measured for current in the $ab$ plane (Fig. 10) increases almost linearly with temperature and indicates metallic behavior of the compound ($\rho_{300\,\mathrm{K}} = 136\ \mu\Omega$ cm). The residual resistance ratio RRR $\approx 3.8$ indicates a fair quality of the specimen and the residual resistance is already reached at $\approx 13$ K. Interestingly, below this temperature $\rho(T)$ increase slightly (by $\approx 0.1$ % of $\rho_0$). The magnetoresistance (MR, Fig. 10 inset) is very small and positive for high $T$. Surprisingly, for $T = 2.0$ K it is negative and quite strong ($-1.7$ % at $\mu_0H = 9$ T). This might indicate the damping of an additional scattering mechanism at very low temperatures compared to the $T_N$. The origin of both the upturn of $\rho(T)$ below 13 K and of the negative MR might be due to a Kondo-hole effect. Nonmagnetic atoms replacing magnetic Cr in the AFM ordered lattice can give rise to a Kondo-like upturn of resistivity at low temperatures. This scattering is weakened by the application of a magnetic field resulting in a negative MR proportional to the field. The Hall resistivity curves $\rho_{ab}(H)$ are linear, the Hall constants are positive and do almost not vary with temperature. This observation is consistent with the hole pocket around the $\Gamma$ point (cf. Fig. 5). Within a one-band model the Hall constant corresponds to a hole density $n_h \approx 1.5\times10^{22}$ cm$^{-3}$ and low mobility ($b_h = 11$ cm$^2$ V$^{-1}$ s$^{-1}$ at $T = 2$ K).

For polycrystalline BaCrFeAs$_2$ (Fig. 10) as well as for a single crystal (not shown), the electrical resistivity is

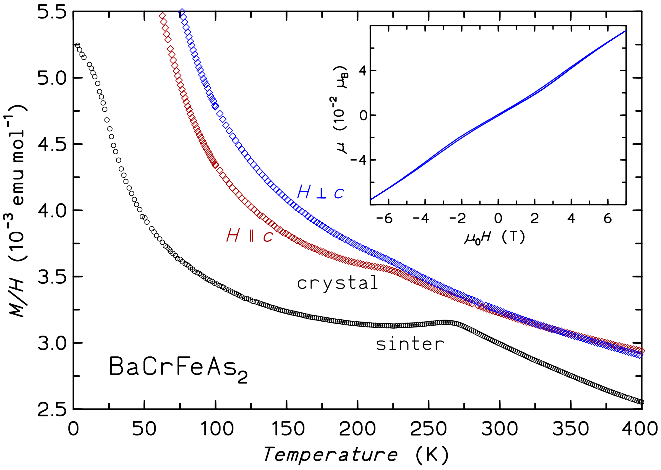

FIG. 9. Magnetic susceptibility of the BaCrFeAs$_2$ sintered sample used for the other measurements (black circles) in a field $\mu_0H = 1$ T. For comparison, the susceptibility of a BaCrFeAs$_2$ crystal (diamonds) with field perpendicular and parallel to the $c$ axis is shown (shifted up by $5\times10^{-4}$ emu mol$^{-1}$). The crystal has a lower Néel temperature. The inset shows the magnetization loop at $T = 2.0$ K.

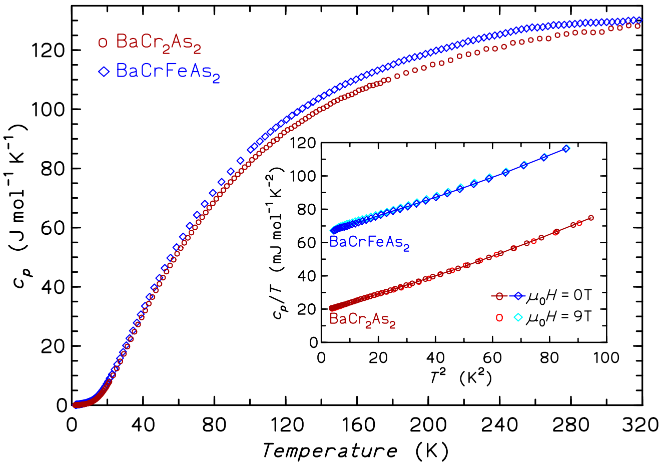

FIG. 11. Molar specific heat $c_p(T)$ of a $BaCr_2As_2$ single crystal (red circles) and of polycrystalline sintered $BaCrFeAs_2$ (blue diamonds). (Inset) $c_p/T$ vs $T^2$ representation for low temperatures. Zero-field data (dark symbols and line) and data in a magnetic field $\mu_0H = 9$ T (light symbols) are shown.

about five time higher. Interestingly, $\rho(T)$ displays only a weak temperature dependence and increases continuously with decreasing $T$. Similar to $BaCr_2As_2$, there is an upturn below a certain temperature (here, $\approx 40$ K). The absence of typical metallic behavior is probably due to scattering of charge carriers on the disordered Cr/Fe species of the $4d$ Wyckoff site. The order of magnitude suggests, however, that $BaCrFeAs_2$ is still a metal. Nominally isoelectronic $BaMn_2As_2$ crystals grown in MnAs flux show an about 100 times higher resistivity [6]. The MR of $BaCrFeAs_2$ is small ($< 0.15$ %) for all temperatures, indicating that magnetic scattering due to the Cr/Fe disorder is unimportant. Also, for $BaCrFeAs_2$, the Hall isotherms $\rho_{xy}(H)$ are linear, however, Hall constants are negative and vary with temperature. They correspond to electron densities $n_e = 8.3\times10^{21}$ cm$^{-3}$ at $T = 300$ K and $1.5\times10^{21}$ cm$^{-3}$ at 2 K with $b_e = 6$ cm$^2$ V$^{-1}$ s$^{-1}$.

The specific heat, $c_p(T)$, of the two compounds is presented in Fig. 11. For $BaCr_2As_2$, no anomalies from transitions are visible up to 320 K. However, $c_p(T)$ for $BaCrFeAs_2$ is larger than that of $BaCr_2As_2$ in the covered temperature range, which might also be due to the Cr/Fe disorder. A very small steplike anomaly can be seen at $\approx 260$ K (barely standing out of the noise). The transition temperature is in agreement with our magnetization and neutron diffraction data (see Sec. III E). The small entropy change connected with this magnetic ordering is due to the low ordered moments of Cr/Fe and the predominantly itinerant character of the magnetic system. The Dulong-Petit limit $c_p = 3nR$ ($R$ = molar gas constant, $n$ = number of atoms) is reached by both compounds at around room temperature.

At low temperatures, the specific heats (see Fig. 11 inset) are well described by $c_p(T) = \gamma T + \beta T^3 + \delta T^5$, where $\gamma$ is the coefficient of the linear term $\gamma T$ (usually assigned to conduction electrons) and $\beta T^3$ and $\delta T^5$ are the first two terms due to the harmonic theory of lattice specific heat. For $BaCr_2As_2$ ($BaCrFeAs_2$), least-squares fits in the range 1.9–7 K result in $\gamma = 18.8$ (64.9) mJ mol$^{-1}$ K$^{-1}$, $\beta = 0.51$ (0.56) mJ mol$^{-1}$ K$^{-4}$ corresponding to an initial Debye temperature of 268 (259) K, and $\delta = 0.6$ (0.0) $\mu$J mol$^{-1}$ K$^{-6}$. The $\gamma$ value obtained for $BaCr_2As_2$ is close to the value deduced by Singh *et al.* [35], however, the linear term of $BaCrFeAs_2$ is very large. The $\gamma$ value for $BaCrFeAs_2$ is confirmed through measurements on the single crystal for which we show the susceptibility in Fig. 9. The lattice properties (Debye temperatures) of the two compounds are similar, as expected from the small atomic mass difference of Cr and Fe. Magnetic contributions from AFM spin waves do not play a role due to the high $T_N$.

The linear specific heat contribution is insensitive to magnetic fields (cf. Fig. 11 inset). For $BaCr_2As_2$ in a field $\mu_0H = 9$ T, the linear coefficient $\gamma$ is not changed at all. For $BaCrFeAs_2$ the specific heat increases slightly in $\mu_0H = 9$ T for $T < 5$ K (by maximally 1.8 % at 3.3 K), which might be due to a Schottky-type anomaly due to minor impurities. Thus, the enhanced $\gamma$ values should either not be due to spin fluctuations at all or the spin fluctuations are of too high in energy. Especially $BaCr_2As_2$ has a very high Néel temperature and the fluctuations might not be quenchable by a small field.

### E. Magnetic structures

In order to investigate the magnetic structure of $BaCr_2As_2$ we have collected a powder neutron pattern at 2 K. In comparison to the data collected at 750 K, well above the Néel temperature $T_N = 580$ K, it was shown that magnetic intensities appear at the positions of nuclear Bragg reflections indicating a magnetic structure, which can be described with the propagation vector $\boldsymbol{k} = 0$. This shows that the translation $\boldsymbol{t} = (\frac{1}{2},\frac{1}{2},\frac{1}{2})$ associated with the $I$ cell is not lost. In Fig. 2, it can be seen that the strongest magnetic intensity is observed at $2\theta = 27.4^\circ$, which is the position of the Bragg reflection 101. Strong intensity could be generated at this position using a magnetic structure model, where the chromium atoms in the Wyckoff positions $4d$, located at $(0,\frac{1}{2},\frac{1}{4})$ and $(\frac{1}{2},0,\frac{1}{4})$, are coupled antiparallel. Due to the $I$ centering the operation $\boldsymbol{t} = (\frac{1}{2},\frac{1}{2},\frac{1}{2})$ does not change the direction of the spin. Therefore one finds the spin sequence $+ - + -$ for the Cr atoms in the positions $(0,\frac{1}{2},\frac{1}{4})$, $(\frac{1}{2},0,\frac{1}{4})$, $(\frac{1}{2},0,\frac{3}{4})$, and $(0,\frac{1}{2},\frac{3}{4})$.

Using this structure model, the magnetic structure could be successfully refined, when the magnetic moments are aligned parallel to the $c$ axis. The same type of magnetic ordering is found for $BaMn_2As_2$ and also for the Cr sublattice in $EuCr_2As_2$ [38]. Assuming an additional magnetic component within the $ab$ plane, magnetic intensity should appear at the position of the reflection 002. Magnetic intensity could not be easily determined from the difference patterns collected at 2 and 750 K, in the fully ordered and the paramagnetic state, because the strong structural changes lead to a change of the nuclear intensity of the reflection 002. Therefore we have refined simultaneously the crystal and the magnetic structure at 2 K. The calculated nuclear intensity of the 002 reflection is even slightly larger than the observed one. This clearly indicates the absence of an additional magnetic component within the $ab$ plane, i.e., the absence of any spin canting to the $c$ axis. From the data set collected at 2 K on instrument E9, we finally found for the Cr atoms a magnetic moment of $\mu_{exp} = 1.88(2)\,\mu_B$ resulting in a residual

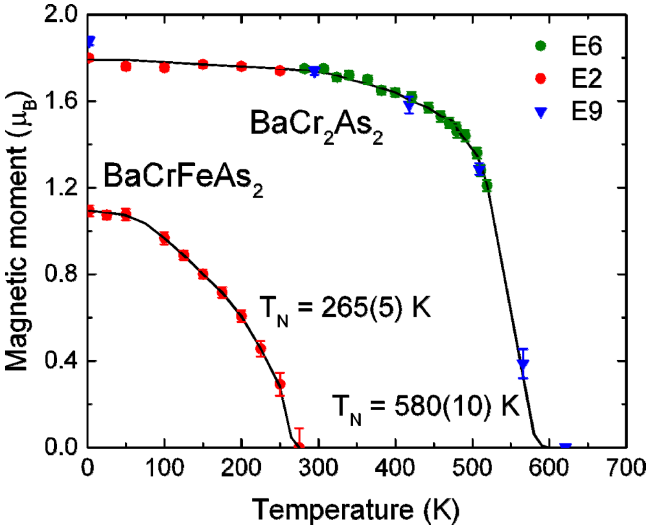

FIG. 12. Temperature dependence of the magnetic moments per transition-metal atom in $BaCr_2As_2$ and $BaCrFeAs_2$ as obtained from powder neutron diffraction data (instruments E2, E6, and E9). Magnetic intensity of Bragg reflections disappears at the Néel temperatures $T_N = 580(10)$ and 265(5) K, respectively.

$R_M = 0.0268$ [defined as $R_M = (\Sigma||I_{obs}| - |I_{calc}||)/\Sigma|I_{obs}|$]. From the data set collected on instrument E2, the magnetic moment $\mu_{exp} = 1.80(2)\,\mu_B$ was found to be slightly smaller (residual $R_M = 0.118$). Moreover, the moment value determined from the E9 data is more reliable, since the overall scale factor could be determined with higher accuracy (a much larger number of nuclear Bragg reflections was available). From the data collected on E2, E6, and E9 we are able to determine the temperature dependence of the magnetic moment up to the Néel temperature $T_N = 580(10)$ K (see Fig. 12). The results from the neutron diffraction experiments compare well with those from magnetization data of the $BaCr_2As_2$ single crystal (Fig. 8). The experimental magnetic Cr moments at 2 K compare reasonably well with the values obtained from our (cf. Table II and previous [35] electronic structure calculations). The experimental Cr moment is even slightly smaller than the calculated moments. This shows that electronic correlation effects reflected in the parameter $U$ of the LDA + $U$ calculations do not play a role as increasing $U$ lead to larger Cr magnetic moments.

Accordingly, we have determined the magnetic structure of $BaCrFeAs_2$. As it can be seen in Fig. 2, the strongest magnetic intensity could also be observed at the position of the reflection 101. The magnetic intensities of $BaCrFeAs_2$ are found to be much weaker than those in $BaCr_2As_2$ indicating that the averaged magnetic moments of the Cr and Fe atoms are strongly reduced. A moment $\mu_{exp} = 1.09(3)\,\mu_B$ was refined resulting in a residual $R_M = 0.068$. The Néel temperature $T_N = 265(5)$ K compares well with the susceptibility data (Fig. 9).

### F. Mössbauer spectroscopy on $BaCrFeAs_2$

Representative $^{57}$Fe Mössbauer spectra of $BaCrFeAs_2$ are shown in Fig. 13. The room-temperature spectrum appears as a broadened line which can be fitted by a quadrupole doublet with an isomer shift $IS$ of 0.44 mm s$^{-1}$ and a quadrupole splitting $QS$ of 0.13 mm s$^{-1}$. By contrast, the spectrum at 5 K features a complex broad pattern which evidences the presence of magnetic hyperfine splitting. The spectrum was fitted by assuming a distribution of hyperfine fields, yielding $IS = 0.59$ mm s$^{-1}$ and a peak hyperfine field $B_{hf} = 5.4$ T. The isomer shifts are slightly larger than those of $BaFe_2As_2$ [52], which adopts the SDW phase below the magnetic ordering temperature. Nevertheless, the local electronic structure is quite similar in the two compounds. Most remarkably, the peak $B_{hf}$ of about 5 T in $BaCrFeAs_2$ is nearly the same as the $B_{hf}$ in the magnetically ordered phases of $BaFe_2As_2$ [52] and LaOFeAs [53]. From the neutron diffraction study, we obtained an average magnetic moment of 1.09 $\mu_B$ per magnetic ion. Assuming that the Cr moment is the same as in $BaCr_2As_2$ (1.8 $\mu_B$) we estimate the iron moment as 0.4 $\mu_B$.

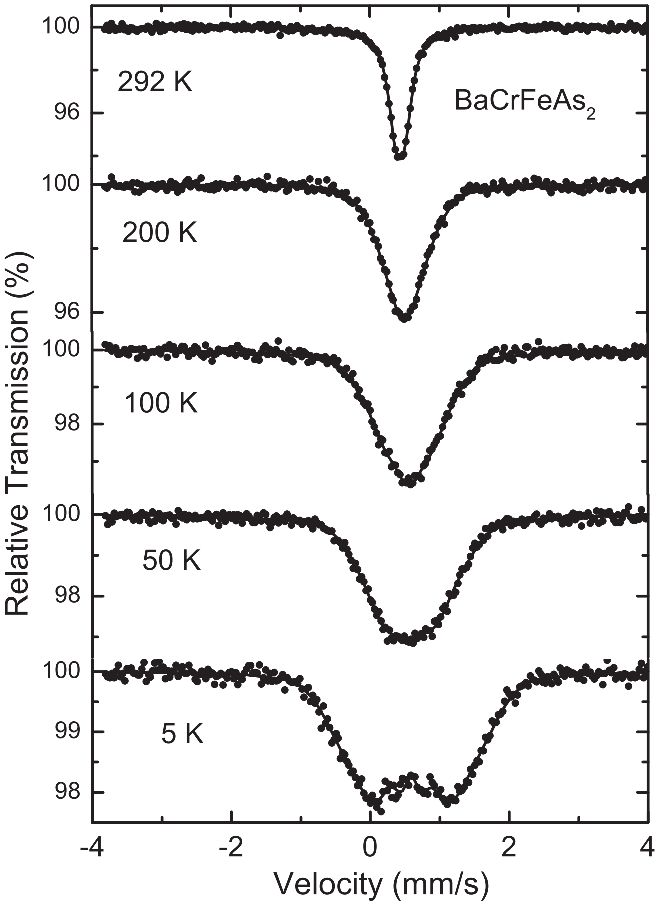

FIG. 13. Mössbauer spectra of $BaCrFeAs_2$ at the indicated temperatures. Dots correspond to the experimental data, solid lines to the best fits.

It has been pointed out that a direct estimation of Fe moments from $B_{hf}$ is questionable due to spin-orbit induced contributions to $B_{hf}$ in the iron pnictides [54]. Nevertheless, a small iron moment is in qualitative agreement with the small $B_{hf}$ for $BaCrFeAs_2$. A similarly small iron moment of 0.4 $\mu_B$ was reported for LaOFeAs [55], whereas a larger moment of 0.9 $\mu_B$ was derived for $BaFe_2As_2$ [16]. The spectra of $BaCrFeAs_2$ are, however, much less resolved than those of $BaFe_2As_2$ and LaOFeAs which reflects the Fe-Cr disorder in

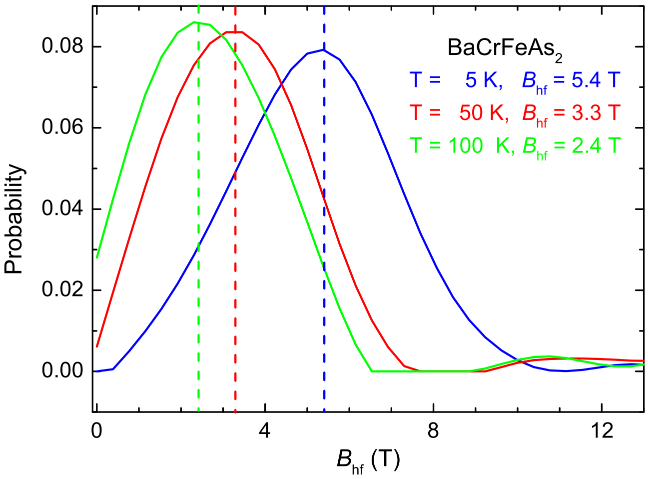

FIG. 14. Hyperfine field distributions in the low-temperature range which were extracted from Mössbauer spectra of BaCrFeAs$_2$. The dashed lines indicate the positions of the peak hyperfine fields given in the figure.

the present material giving rise to a broad $B_{\mathrm{hf}}$ distribution. Both, neutron diffraction and Mössbauer data confirm that Fe and Cr atoms are disordered, while some previous electronic structure calculations assumed an ordered arrangement [6,36]. A large ordered Fe moment of 2.5–2.6 $\mu_{\mathrm{B}}$ predicted from the electronic structure calculations for atomically ordered BaCrFeAs$_2$ (Ref. [36] and Table III) is incompatible with the neutron diffraction and the Mössbauer data.

Indications for an unusual behavior of the Fe moments is obtained from the temperature dependence of $B_{\mathrm{hf}}$. With increasing temperature a pronounced decrease in hyperfine splitting is apparent even in the temperature region 5–100 K (Fig. 13), which is unexpected as the Néel temperature is much higher (265 K). At 100 K, the $B_{\mathrm{hf}}$ distribution even extends down to 0 T (Fig. 14) indicating that a fraction of the iron atoms is already nonmagnetic. These observations are in contrast to the behavior of BaFe$_2$As$_2$ where in this temperature range only a minor reduction of $B_{\mathrm{hf}}$ was observed although $T_{\mathrm{N}}$ is considerably smaller ($\approx$ 140 K) [52]. The strong decrease of the peak $B_{\mathrm{hf}}$ from 5.4 T at 5 K to 2.4 T at 100 K is also in sharp contrast to the temperature dependence of the total magnetic moments derived from neutron diffraction (Fig. 12).

A possible scenario is that the Fe moments do not participate in the $G$-type AFM structure and rather freeze in the low temperature range, which is consistent with the fact that no anomaly is apparent in the temperature dependence of the moments between 2 and 100 K. The formation of the $G$-type AFM order then is still driven by the large Cr moments. Further on, the upturn in the susceptibility $\chi(T)$ below $T_{\mathrm{N}} = 265$ K (Fig. 9), which is in contrast to the behavior of BaCr$_2$As$_2$, is a further indication that the iron moments are at least partially disordered. As demonstrated above electronic structure calculations of atomically disordered BaCrFeAs$_2$ starting with zero Fe moment result in a stable solution with $\mu_{\mathrm{Fe}} \sim 0$ and $\mu_{\mathrm{Cr}} = 2.76\ \mu_{\mathrm{B}}$. The resulting average moment of 1.38 $\mu_{\mathrm{B}}$ per formula unit is not too far from the experimental moment of 1.09 $\mu_{\mathrm{B}}$. The mismatch of the Fe moments with $G$-type antiferromagnetism explains why $T_{\mathrm{N}}$ in Fe-substituted BaCr$_2$As$_2$ decreases drastically from 580 K in the parent compound to $\approx$ 50 K for an iron content of about 70% where finally the $G$-type order becomes unstable and is replaced by the SDW structure [34]. At higher temperature, the hyperfine splitting further decreases and for $T \geqslant 200$ K essentially a broad unstructured line is found. In this temperature range the Fe atoms are possibly polarized by the Cr moments. Above 260 K, only minor changes in line broadening occur which compares well with $T_{\mathrm{N}} = 265$ K.

## IV. CONCLUSIONS

We have studied in detail the structural, electronic, and magnetic properties of BaCr$_2$As$_2$ and BaCrFeAs$_2$. BaCr$_2$As$_2$ as well as LaOCrAs [26,27] have been discussed recently in connection with the Mott scenario (see Sec. I) of transition-metal arsenide superconductivity (sc). Our powder neutron diffraction studies verify that BaCr$_2$As$_2$ adopts the theoretically predicted $G$-type AFM order at $T_{\mathrm{N}} = 580$ K and an ordered moment $\mu_{\mathrm{Cr}} = 1.9\ \mu_{\mathrm{B}}$ at 2 K. Evidence for magnetostructural coupling effects was found and it remains to be clarified whether this reflects some type of electronic instability. The experimental magnetic Cr moment agrees well with LDA electronic structure calculations, whereas incorporation of electron correlation within the LDA + $U$ scheme leads to Cr moments, which are too high. $T_{\mathrm{N}}$ is 1/3 lower than the ordering temperature calculated within mean-field approximation, underlining the somewhat two-dimensional character of the magnetic system.

BaCrFeAs$_2$ still adopts this $G$-type AFM structure but the ordering temperature is less than half of that of BaCr$_2$As$_2$. The small average moment $\mu_{\mathrm{Cr/Fe}} \approx 1.1\ \mu_{\mathrm{B}}$ in connection with the small hyperfine field from Mössbauer spectra is in agreement with the results of our calculations for atomically disordered BaCrFeAs$_2$ and an Fe moment $\mu_{\mathrm{Fe}} \sim 0$. The Néel temperature calculated within mean-field approximation is in good agreement with the experimental value (260 and 265 K, respectively). Also the average Cr/Fe moment is in fair agreement with the calculation (2.76 $\mu_{\mathrm{B}}$, distributed on two atoms). These findings, together with an anomalous temperature dependence of the hyperfine field, indicate that the small Fe moments are not incorporated into the $G$-type AFM order. Thus it may be conjectured that Fe favors the stripe-type and Cr the checkerboard-type spin fluctuations, the latter being considered to be detrimental to sc [4]. In case of electron pairing mediated by spin-fluctuations this finding would be in agreement with the fact that so far no sc was observed for BaCr$_2$As$_2$ or Cr-substituted BaFe$_2$As$_2$. Similarly, no superconductivity was found in Mn-substituted BaFe$_2$As$_2$, where the pure Mn compound BaMn$_2$As$_2$ adopts a stable $G$-type AFM order as well. Accordingly, not only the doping level but also the type of spin fluctuations has to be considered for predictions of new sc compositions.

Both BaCr$_2$As$_2$ and BaCrFeAs$_2$ are metals. The linear specific heat (Sommerfeld) coefficients $\gamma$ are much larger than expected from band theory, by a factor of 2.4 for BaCr$_2$As$_2$ and a huge factor of 5.5 for BaCrFeAs$_2$. The discrepancies for both compounds cannot be resolved by reasonable strengths of correlations. However, it seems that for BaCrFeAs$_2$ the disorder of the magnetic Cr and Fe atoms to some extent additionally boosts the $\gamma$ value.

Our findings may be compared with results for the better investigated Mn 122 system. In contrast to $BaCr_2As_2$ $BaMn_2As_2$ is semiconducting [5–9]. The nominal $3d^5$ compound has a Néel temperature which is slightly higher than that of $BaCr_2As_2$. It is possible to induce a metallic state in $BaMn_2As_2$ by application of pressure [56] or by hole-doping with as little as 1.6 % of K [57]. In this metallic state $Ba_{1-x}K_xMn_2As_2$ is still $G$-type ordered [58] and is thus similar to $BaCr_2As_2$. But there is one important difference, the Sommerfeld $\gamma$ in the metallic Mn system is smaller (8.4 mJ $\mathrm{mol}^{-1}\,\mathrm{K}^{-1}$ for $x = 0.05$ [57]) than in $BaCr_2As_2$. This suggests that electronic correlations are weak in the $BaMn_2As_2$ materials. A recent photoemission (ARPES) study corroborates that there is almost no band renormalization with respect to the DFT-based band structure in $BaMn_2As_2$ [9]. In order to shed more light on the development of electronic correlations in the 122 arsenide family, we recently performed an ARPES study on $BaCr_2As_2$ [59].

For $Ba_{1-x}K_xMn_2As_2$, the Néel temperature and the ordered Mn moment remain almost constant up to high substitution levels ($x \leqslant 0.4$) [58]. In contrast, in the substitution series $BaFe_{2-x}Mn_xAs_2$ for a low Mn substitution level $x = 0.15$ a clear competition between stripe-type and checkerboard-type spin fluctuations could be observed by inelastic neutron scattering [60], quite similar to the $BaCr_{2-x}Fe_xAs_2$ series [34]. For $BaFe_{2-x}Mn_xAs_2$, a miscibility gap prevents the synthesis of single-phase material for Mn contents $x > 0.24$ [61].

Although both modified $BaMn_2As_2$-based ($3d^5$) materials [56–58] as well as $BaCr_2As_2$ are AFM-ordered metals, until now there are no ways known to obtain superconductors based on these materials. The partial substitution of Ba by K in $BaCr_2As_2$ showed to be unsuccessful, but resulted in the discovery of sc $K_2Cr_3As_3$ [31,32]. Another way to possibly generate sc in Mn or Cr-based 122 or 1111-type arsenides is the application of high pressure. With high pressure, in transition-metal arsenides structural instabilities come into play. We have undertaken a structural and electrical transport study on one of our $BaCr_2As_2$ crystals under high pressure, the results of which have been reported recently [62].

## ACKNOWLEDGMENT

We thank Ralf Koban for assistance and Igor Veremchuk for spark plasma sintering of a sample. M.G. acknowledges support of US-NSF-DMR 1507252 Grant.

---

[1] E. Bascones, B. Valenzuela, and M. J. Calderón, Magnetic interactions in iron superconductors: A review, C. R. Phys. **17**, 36 (2016).

[2] P. Dai, Antiferromagnetic order and spin dynamics in iron-based superconductors, Rev. Mod. Phys. **87**, 855 (2015).

[3] Q. Si, R. Yu, and E. Abrahams, High temperature superconductivity in iron pnictides and chalcogenides, Nat. Rev. Mater. **1**, 16017 (2016).

[4] R. M Fernandes and A. J Millis, Suppression of Superconductivity by Néel-Type Magnetic Fluctuations in the Iron Pnictides, Phys. Rev. Lett. **110**, 117004 (2013).

[5] J. An, A. S. Sefat, D. J. Singh, and M.-H. Du, Electronic structure and magnetism in $BaMn_2As_2$ and $BaMn_2Sb_2$, Phys. Rev. B **79**, 075120 (2009).

[6] Y. Singh, A. Ellern, and D. C. Johnston, Magnetic, transport, and thermal properties of single crystals of the layered arsenide $BaMn_2As_2$, Phys. Rev. B **79**, 094519 (2009).

[7] Y. Singh, M. A. Green, Q. Huang, A. Kreyssig, R. J. McQueeney, D. C. Johnston, and A. I. Goldman, Magnetic order in $BaMn_2As_2$ from neutron diffraction measurements, Phys. Rev. B **80**, 100403 (2009).

[8] D. C. Johnston, R. J. McQueeney, B. Lake, A. Honecker, M. E. Zhitomirsky, R. Nath, Y. Furukawa, V. P. Antropov, and Y. Singh, Magnetic exchange interactions in $BaMn_2As_2$: A case study of the $J_1 - J_2 - J_c$ Heisenberg model, Phys. Rev. B **84**, 094445 (2011).

[9] W.-L. Zhang, P. Richard, A. v. Roekeghem, S.-M. Nie, N. Xu, P. Zhang, H. Miao, S.-F. Wu, J.-X. Yin, B. B. Fu, L.-Y. Kong, T. Qian, Z.-J. Wang, Z. Fang, A. S. Sefat, S. Biermann, and H. Ding, Angle-resolved photoemission observation of Mn-pnictide hybridization and negligible band structure renormalization in $BaMn_2As_2$ and $BaMn_2Sb_2$, Phys. Rev. B **94**, 155155 (2016).

[10] A. Beleanu, J. Kiss, G. Kreiner, C. Köhler, L. Müchler, W. Schnelle, U. Burkhardt, S. Chadov, S. Medvediev, D. Ebke, C. Felser, G. Cordier, B. Albert, A. Hoser, F. Bernardi, T. I. Larkin, D. Pröpper, A. V. Boris, and B. Keimer, Large resistivity change and phase transition in the antiferromagnetic semiconductors LiMnAs and LaOMnAs, Phys. Rev. B **88**, 184429 (2013).

[11] S. Dong, W. Li, X. Huang, and E. Dagotto, First principles study of the magnetic properties of LaOMnAs, J. Appl. Phys. **115**, 17D723 (2014).

[12] P. Dai, J. Hu, and E. Dagotto, Magnetism and its microscopic origin in iron-based high-temperature superconductors, Nat. Phys. **8**, 709 (2012).

[13] N. Mannella, The magnetic moment enigma in Fe-based high temperature superconductors, J. Phys.: Condens. Matter **26**, 473202 (2014).

[14] S. Backes, H. O. Jeschke, and R. Valenti, Microscopic nature of correlations in multiorbital $AFe_2As_2$ ($A =$ K, Rb, Cs): Hund's coupling versus Coulomb repulsion, Phys. Rev. B **92**, 195128 (2015).

[15] M. Rotter, M. Tegel, D. Johrendt, I. Schellenberg, W. Hermes, and R. Pöttgen, Spin-density-wave anomaly at 140 K in the ternary iron arsenide $BaFe_2As_2$, Phys. Rev. B **78**, 020503 (2008).

[16] Q. Huang, Y. Qiu, W. Bao, M. A. Green, J. W. Lynn, Y. C. Gasparovic, T. Wu, G. Wu, and X. H. Chen, Neutron-Diffraction Measurements of Magnetic Order and a Structural Transition in the Parent $BaFe_2As_2$ Compound of FeAs-Based High-Temperature Superconductors, Phys. Rev. Lett. **101**, 257003 (2008).

[17] G.-F. Chen, Z. Li, G. Li, W.-Z. Hu, J. Dong, J. Zhou, X.-D. Zhang, P. Zheng, N.-L. Wang, and J.-L. Luo, Superconductivity in hole-doped $(Sr_{1-x}K_x)Fe_2As_2$, Chin. Phys. Lett. **25**, 3403 (2008).

[18] K. Sasmal, B. Lv, B. Lorenz, A. M. Guloy, F. Chen, Y.-Y. Xue, and C.-W. Chu, Superconducting Fe-Based Compounds $(A_{1-x}Sr_xFe_2As_2$ with $A = $ K and Cs with Transition Temperatures up to 37 K, Phys. Rev. Lett. **101**, 107007 (2008).

[19] P. L. Alireza, Y. T. Chris Ko, J. Gillett, C. M. Petrone, J. M. Cole, G. G. Lonzarich, and S. E. Sebastian, Superconductivity up to 29 K in $SrFe_2As_2$ and $BaFe_2As_2$ at high pressures, J. Phys.: Condens. Matter **21**, 012208 (2008).

[20] A. S. Sefat, R. Jin, M. A. McGuire, B. C. Sales, D. J. Singh, and D. Mandrus, Superconductivity at 22 K in Co-Doped $BaFe_2As_2$ Crystals, Phys. Rev. Lett. **101**, 117004 (2008).

[21] A. Leithe-Jasper, W. Schnelle, C. Geibel, and H. Rosner, Superconducting State in $SrFe_{2-x}Co_xAs_2$ by Internal Doping of the Iron Arsenide Layers, Phys. Rev. Lett. **101**, 207004 (2008).

[22] W. Schnelle, A. Leithe-Jasper, R. Gumeniuk, U. Burkhardt, D. Kasinathan, and H. Rosner, Substitution-induced superconductivity in $SrFe_{2-x}Ru_xAs_2$ $(0 \leqslant x \leqslant 2)$, Phys. Rev. B **79**, 214516 (2009).

[23] D. Kasinathan, A. Ormeci, K. Koch, U. Burkhardt, W. Schnelle, A. Leithe-Jasper, and H. Rosner, $AFe_2As_2$ (A= Ca, Sr, Ba, Eu) and $SrFe_{2-x}TM_xAs_2$ (TM = Mn, Co, Ni): Crystal structure, charge doping, magnetism and superconductivity, New J. Phys. **11**, 025023 (2009).

[24] O. Moze, M. Hofmann, J. M. Cadogan, K. H. J. Buschow, and D. H. Ryan, Magnetic order in $RCr_2Si_2$ intermetallics, Eur. Phys. J. B **36**, 511 (2003).

[25] H. Ishida and A. Liebsch, Fermi-liquid, non-Fermi-liquid, and Mott phases in iron pnictides and cuprates, Phys. Rev. B **81**, 054513 (2010).

[26] M. Edelmann, G. Sangiovanni, M. Capone, and L. de'Medici, Chromium analogues of iron-based superconductors, arXiv:1610.10054.

[27] J. M. Pizarro, M. J. Calderón, J. Liu, M. C. Muñoz, and E. Bascones, Strong correlations and the search for high-$T_c$ superconductivity in chromium pnictides and chalcogenides, Phys. Rev. B **95**, 075115 (2017).

[28] W. Wu, J. Cheng, K. Matsubayashi, P. Kong, F. Lin, C. Jin, N. Wang, Y. Uwatoko, and J. Luo, Superconductivity in the vicinity of antiferromagnetic order in CrAs, Nat. Commun. **5**, 5508 (2014).

[29] H. Kotegawa, S. Nakahara, H. Tou, and H. Sugawara, Superconductivity of 2.2 K under pressure in helimagnet CrAs, J. Phys. Soc. Jpn. **83**, 093702 (2014).

[30] J.-G. Cheng, K. Matsubayashi, W. Wu, J. P. Sun, F. K. Lin, J. L. Luo, and Y. Uwatoko, Pressure Induced Superconductivity on the Border of Magnetic Order in MnP, Phys. Rev. Lett. **114**, 117001 (2015).

[31] J.-K. Bao, J.-Y. Liu, C.-W. Ma, Z.-H. Meng, Z.-T. Tang, Y.-L. Sun, H.-F. Zhai, H. Jiang, H. Bai, C.-M. Feng, Z.-A. Xu, and G.-H. Cao, Superconductivity in Quasi-One-Dimensional $K_2Cr_3As_3$ with Significant Electron Correlations, Phys. Rev. X **5**, 011013 (2015).

[32] G.-H. Cao, J.-K. Bao, Z.-T. Tang, Y. Liu, and H. Jiang, Peculiar properties of $Cr_3As_3$-chain-based superconductors, Philos. Mag. B **97**, 591 (2017).

[33] A. S. Sefat, D. J. Singh, L. H. VanBebber, Y. Mozharivskyj, M. A. McGuire, R. Jin, B. C. Sales, V. Keppens, and D. Mandrus, Absence of superconductivity in hole-doped $BaFe_{2-x}Cr_xAs_2$ single crystals, Phys. Rev. B **79**, 224524 (2009).

[34] K. Marty, A. D. Christianson, C. H. Wang, M. Matsuda, H. Cao, L. H. VanBebber, J. L. Zarestky, D. J. Singh, A. S. Sefat, and M. D. Lumsden, Competing magnetic ground states in nonsuperconducting $Ba(Fe_{1-x}Cr_x)_2As_2$ as seen via neutron diffraction, Phys. Rev. B **83**, 060509 (2011).

[35] D. J. Singh, A. S. Sefat, M. A. McGuire, B. C. Sales, D. Mandrus, L. H. VanBebber, and V. Keppens, Itinerant antiferromagnetism in $BaCr_2As_2$: Experimental characterization and electronic structure calculations, Phys. Rev. B **79**, 094429 (2009).

[36] S.-J. Hu and X. Hu, Half-metallic antiferromagnet $BaCrFeAs_2$, J. Phys. Chem. C **114**, 11614 (2010).

[37] U. B. Paramanik, R. Prasad, C. Geibel, and Z. Hossain, Itinerant and local-moment magnetism in $EuCr_2As_2$ single crystals, Phys. Rev. B **89**, 144423 (2014).

[38] S. Nandi, Y. Xiao, N. Qureshi, U. B. Paramanik, W. T. Jin, Y. Su, B. Ouladdiaf, Z. Hossain, and Th. Brückel, Magnetic structures of the Eu and Cr moments in $EuCr_2As_2$: Neutron diffraction study, Phys. Rev. B **94**, 094411 (2016).

[39] J. Rodríguez-Carvajal, Recent advances in magnetic structure determination by neutron powder diffraction, Physica B: Condens. Matter **192**, 55 (1993).

[40] V. F. Sears, in *International Tables for Crystallography*, edited by A. J. C. Wilson (Kluwer, Dordrecht, 1995), Vol. C, p. 383.

[41] P. J. Brown, in *International Tables for Crystallography*, edited by A. J. C. Wilson (Kluwer, Dordrecht, 1995), Vol. C, p. 391.

[42] MOSSWINN 4.0. http://mosswinn.com.

[43] P. Blaha, K. Schwarz, and P. Sorantin, Full-potential, linearized augmented plane wave programs for crystalline systems, Comput. Phys. Commun. **59**, 399 (1990).

[44] K. Schwarz and P. Blaha, Solid state calculations using WIEN2k, Comput. Mater. Sci. **28**, 259 (2003).

[45] P. Blaha, K. Schwarz, G. K. H. Madsen, D. Kvasnicka, and J. Luitz, *WIEN2k, an Augmented Plane Wave + Local Orbitals Program for Calculating Crystal Properties – Revised Edition 14.2* (Karlheinz Schwarz, Techn. Universitaet Wien, Wien, Austria, 2014).

[46] H. Ebert, Fully relativistic band structure calculations for magnetic solids - formalism and application, in *Electronic Structure and Physical Properties of Solids. The Use of the LMTO Method*, edited by H. Dreysse, Lecture Notes in Physics Vol. 535 (Springer-Verlag, Berlin, Heidelberg, 1999), p. 191.

[47] H. Ebert, D. Ködderitzsch, and J. Minar, Calculating condensed matter properties using the KKR-Green's function method: Recent developments and applications, Rep. Prog. Phys **74**, 096501 (2011).

[48] J. P. Perdew, K. Burke, and M. Ernzerhof, Generalized Gradient Approximation Made Simple, Phys. Rev. Lett. **77**, 3865 (1996).

[49] M. Pfisterer and G. Nagorsen, Zur Struktur ternärer Übergangsmetallarsenide, Z. Naturforsch. B **35b**, 703 (1980); Bindungsverhältnisse und magnetische Eigenschaften ternärer Arsenide $ET_2As_2$, *ibid.*, **38b**, 811 (1983).

[50] W. Jeitschko, U. Meisen, M. H. Möller, and M. Reehuis, Über $LaCo_2P_2$ und andere neue Verbindungen mit $ThCr_2Si_2$- und $CaBe_2Ge_2$ Struktur, Z. Anorg. Allg. Chem. **527**, 73 (1985).

[51] H. Boller and A. Kallel, First order crystallographic and magnetic phase transition in CrAs, Solid State Commun. **9**, 1699 (1971).

[52] A. Błachowski, K. Ruebenbauer, J. Żukrowski, K. Rogacki, Z. Bukowski, and J. Karpinski, Shape of spin density wave versus temperature in $AFe_2As_2$ (A = Ca, Ba, Eu): A Mössbauer study, Phys. Rev. B **83**, 134410 (2011).

[53] M. A. McGuire, A. D. Christianson, A. S. Sefat, B. C. Sales, M. D. Lumsden, R. Jin, E. A. Payzant, D. Mandrus, Y. Luan, V. Keppens, V. Varadarajan, J. W. Brill, R. P. Hermann, M. T. Sougrati, F. Grandjean, and G. J. Long, Phase transitions in LaFeAsO: Structural, magnetic, elastic, and transport properties, heat capacity and Mössbauer spectra, Phys. Rev. B **78**, 094517 (2008).

[54] G. Derondeau, J. Minár, and H. Ebert, Hyperfine fields in the $BaFe_2As_2$ family and their relation to the magnetic moment, Phys. Rev. B **94**, 214508 (2016).

[55] C. de la Cruz, Q. Huang, J. W. Lynn, J. Li, W. Ratcliff II, J. L. Zarestky, H. A. Mook, G. F. Chen, J. L. Luo, N. L. Wang, and P. Dai, Magnetic order close to superconductivity in the iron-based layered $LaO_{1-x}F_xFeAs$ systems, Nature (London) **453**, 899 (2008).

[56] A. T. Satya, A. Mani, A. Arulraj, N. V. Chandra Shekar, K. Vinod, C. S. Sundar, and A. Bharathi, Pressure-induced metallization of $BaMn_2As_2$, Phys. Rev. B **84**, 180515(R) (2011).

[57] A. Pandey, R. S. Dhaka, J. Lamsal, Y. Lee, V. K. Anand, A. Kreyssig, T. W. Heitmann, R. J. McQueeney, A. I. Goldman, B. N. Harmon, A. Kaminski, and D. C. Johnston, $Ba_{1-x}K_xMn_2As_2$: An Antiferromagnetic Local-Moment Metal, Phys. Rev. Lett. **108**, 087005 (2012).

[58] J. Lamsal, G. S. Tucker, T. W. Heitmann, A. Kreyssig, A. Jesche, A. Pandey, W. Tian, R. J. McQueeney, D. C. Johnston, and A. I. Goldman, Persistence of local-moment antiferromagnetic order in $Ba_{1-x}K_xMn_2As_2$, Phys. Rev. B **87**, 144418 (2013).

[59] J. Nayak, K. Filsinger, G. H. Fecher, S. Chadov, J. Minár, E. E. D. Rienks, B. Büchner, J. Fink, and C. Felser, Observation of a remarkable reduction of correlation effects in $BaCr_2As_2$ by ARPES, arXiv:1701.06108.

[60] G. S. Tucker, D. K. Pratt, M. G. Kim, S. Ran, A. Thaler, G. E. Granroth, K. Marty, W. Tian, J. L. Zarestky, M. D. Lumsden, S. L. Bud'ko, P. C. Canfield, A. Kreyssig, A. I. Goldman, and R. J. McQueeney, Competition between stripe and checkerboard magnetic instabilities in Mn-doped $BaFe_2As_2$, Phys. Rev. B **86**, 020503(R) (2012).

[61] A. Pandey, V. K. Anand, and D. C. Johnston, Large miscibility gap in the $Ba(Mn_xFe_{1-x})_2As_2$ system, Phys. Rev. B **84**, 014405 (2011).

[62] P. G. Naumov, K. Filsinger, O. I. Barkalov, G. H. Fecher, S. A. Medvedev, and C. Felser, Pressure induced transition to the collapsed tetragonal phase in $BaCr_2As_2$, Phys. Rev. B **95**, 144106 (2017).